Role of Entropy in the Expulsion of Dopants from Optically Trapped Colloidal Assemblies

Hreedish Kakoty,[1] Rajarshi Banerjee,[2] Chandan Dasgupta,[2] and Ambarish Ghosh[1,3,4,*]
[1]Department of Physics, Indian Institute of Science, Bangalore 560012, India
[2]Centre for Condensed Matter Theory, Department of Physics, Indian Institute of Science, Bangalore 560012, India
[3]Centre for Nano Science and Engineering, Indian Institute of Science, Bangalore 560012, India
[4]Department of Electrical Communication Engineering, Indian Institute of Science, Bangalore 560012, India
(Received 8 August 2016; revised manuscript received 13 October 2016; published 16 December 2016)

Controlling an assembly of colloidal particles under external forces can be helpful in developing soft nanomaterials with novel functionalities. How external impurities organize within such confined systems is of fundamental and technological interest, especially when the system sizes are so small that even a single dopant can interact with an appreciable fraction of the system. To address this question, we use a defocused laser beam to form two-dimensional colloidal crystallites containing foreign dopants. Our studies reveal a surprising position dependence in the fate of dopants getting either spontaneously expelled or permanently internalized within the crystallite. This phenomenon arises due to the subtle interplay between the effects of external confinement and the role of entropy in the thermodynamics of small assemblies of interacting particles.

DOI: 10.1103/PhysRevLett.117.258002

Externally controlled assemblies of interacting particles can be encountered in a variety of systems, including electrons in mesoscale helium dimples [1] and bubbles [2], dusty plasma [3], laser-cooled ions in traps [4], and colloidal dispersions under applied fields [5–7]. Among these, suspensions of colloidal particles are especially attractive as model systems to understand the role of interparticle interactions and external fields. For example, it is possible to apply an external magnetic field [8] or change the *p*H [9] of the medium to tune the colloidal interactions. The external force can also be used to drive the system out of equilibrium in a well-controlled manner [10], which can aid in gaining a fundamental understanding of nonequilibrium phenomena.

Although there have been previous studies on the role of defects [11–17] on the nucleation, growth, and overall functionality of colloidal assemblies, the key question addressed here is fundamentally different: How do externally injected impurities or dopants organize within confined colloidal clusters, in particular, small crystallites? Somewhat relevant to this question is the past theoretical investigation of a finite cluster of charged particles confined in a parabolic trap. According to Drocco *et al.* [18], in a cluster of charged particles of two species with Coulomb-like interparticle interactions, particles with a higher charge are always positioned off center. Extending the analysis on the same system, Nelissen, Partoens, and Peeters [19] found that the position of a defect particle can be anywhere, depending on its mass and charge. Although experimental realizations of such systems are scarce, one attempt with magnetically rotated millimeter-sized disks revealed a self-organization of smaller disks around a larger disk at the center [20].

Our experimental system consists of a collection of colloids and a dopant in a highly configurable confinement potential, formed using a defocused optical tweezer. This relatively unknown technique was first introduced by Vossen, Plaisier, and van Blaaderen [21] and recently mentioned by Williams *et al.* [22], who referred to this method as an optical bowl. By varying the power and level of defocusing, colloidal assemblies of different sizes and phases (liquidlike or crystalline) could be formed. Most importantly, we have studied the dynamics of foreign dopants, in the form of particles of different shapes and sizes, injected into the crystallites. The striking result obtained here was the ability of the finite-sized colloidal clusters to expel or internalize a foreign dopant depending on its initial position. This surprising phenomenon could be explained from our simulation results, which showed that the fate of a dopant is governed to a large extent by the entropy of the system, which becomes increasingly important as the size of the crystallite is reduced.

The finite-sized colloidal assembly, consisting of 1 μm polystyrene particles dispersed in deionized water, was formed with a single laser beam [see the schematic in Fig. 1(a)] at 1070 nm focused at a plane (along $\hat{Z}$) higher than the plane of observation (XY) inside a microfluidic chamber made of glass. The colloidal layer was effectively two-dimensional, whose Z position was determined by four counteracting forces, scattering, and gradient forces along $\hat{Z}$ from the laser beam pushing the particles upward balanced by the downward repulsion from the charged glass surface and gravity. In configurations where the Z components of the scattering and gradient forces were in opposite directions, no stable trapping could be observed. The planar confinement of the particles was achieved by the component of the gradient force along the XY plane generated by the converging beam and was strong enough to suppress the out-of-plane fluctuations of the trapped beads to a good degree. We show the formation of the colloidal assembly in Movies M1 and M2; details are available in Supplemental Material, Sec. I [23].

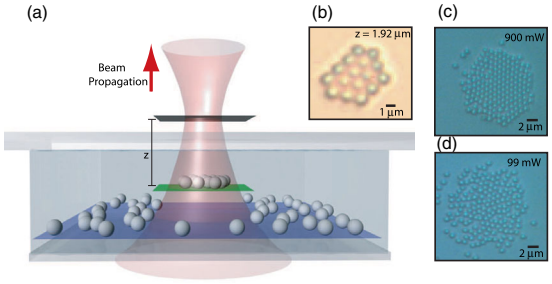

FIG. 1. (a) Schematic of the experimental setup: laser beam focused at a plane higher (along $\hat{Z}$) than the plane of observation containing the colloidal assembly. The confinement along $\hat{Z}$ was obtained due to the balance of forces described in the text, resulting in a finite-sized two-dimensional colloidal cluster. (b), (c) Controlling the size of the colloidal assembly by focusing the laser beam at various distances above the sample plane, $z = 1.9$ and 6.4 μm, respectively. (d) Reducing the laser power to 99 mW while focusing at the same position ($z = 6.4$ μm) results in a disordered (liquidlike) assembly of the same size as the crystallite of (c).

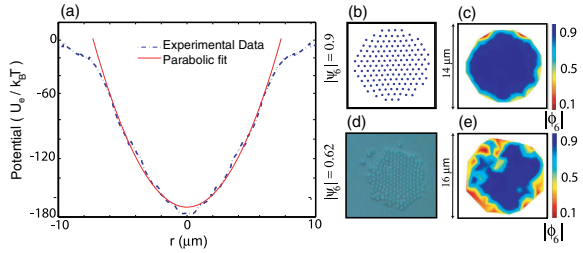

FIG. 2. (a) Experimental measurement of the trapping potential as a function of radial distance, along with a parabolic fit at $z = 6.4$ μm and laser power 225 mW. (b),(d) Snapshots of simulated and experimental crystallites and their corresponding $|\psi_6|$. (c),(e) Local bond-orientational order parameter $|\phi_6|$ for the crystals shown in (b) and (d), respectively.

The size and strength of the optical trap could be controlled by varying the laser power and by moving the focal plane in the $\hat{Z}$ direction (see Supplemental Material, Sec. II [23]). This is shown in Figs. 1(b)–1(d), where we show examples of colloidal assemblies of different sizes as well as different phases (liquidlike or crystalline).

Next, we measure the strength and spatial variation of the trapping potential formed by the laser beam, which was necessary to develop a numerical model. We describe the critical steps here; for more details, see Supplemental Material, Sec. III [23]. We imaged the trajectory of a particle falling into the center of the trap starting from an initial position approximately a few microns off center. Denoting by (r, θ) the instantaneous position of the particle with respect to the center of the trap and its instantaneous velocity in the XY plane by $\vec{v}(r, \theta)$, the trapping potential could be estimated from $U_e(r, \theta) = -\int_{\infty}^{r} \gamma \vec{v}(r', \theta) \cdot \vec{dr}'$, where γ is the drag coefficient of the particle. The acceleration of the particle was neglected, because the Reynolds number was estimated to be small ($\leq 10^{-5}$). The potential was found [see Supplemental Material, Figs. S2(b) and S2(c) [23]] to be approximately circularly symmetric (no θ dependence), which allowed us to obtain $U_e(r)$ by averaging over multiple trajectories. The experimental results are shown in Fig. 2(a). Also shown is a parabolic fit to the experimental data in a region $|r| < 6$ μm, which yielded a spring constant of $K_{\text{trap}} = 2.68 \times 10^{-2}$ pN/μm. As the intensity distribution of the laser was structured and highly non-Gaussian at the sample plane, it is not surprising that the spatial distribution of the potential deviates from a parabola, especially at the edges of the trap. The effective potential would be modified due to light scattering from other particles, but this may be a small effect at right angles to the incident direction. The key point of these measurements was to obtain a realistic estimate of the trapping potential in order to carry out numerical simulations, and, as we discuss later, the exact functional form of the potential does not affect the final conclusions significantly.

In the following discussions, we describe the strength of the trap as a dimensionless parameter U_{trap}/k_BT, where the energy scale $U_{\text{trap}} = \frac{1}{2} K_{\text{trap}} a^2$ is defined as the energy of the trap at a distance equal to the particle diameter. To model a cluster of particles inside the trap, we simulated the dynamics of the particles using the Langevin equation. The effective potential of the ith particle is given by

$$U_i = \sum_{j \neq i} U_{ij}^{\text{int}} + U_i^{\text{ext}},$$

where U_i^{ext} is the external potential due to the optical trap (assumed to be harmonic) and U_{ij}^{int}, the potential due to interparticle interactions, is assumed to have a repulsive screened Coulomb (Yukawa) form:

$$U_{ij}^{\text{int}} = U_0 \frac{\exp(-\lambda r_{ij})}{r_{ij}}.$$

Here, r_{ij} is the center-to-center spacing between particles i and j measured in units of a ($a = 1$ μm is the typical interparticle spacing taken here as the diameter of the particles used in the experiment). The choice of the parameters U_0 and λ was based on a comparison of the results of our simulations with those of previous studies on similar systems, where close-packed crystalline phases were obtained when $\lambda > 5$ and $k_BT/U_0 \exp(-\lambda) < 0.2$ [24–26]. Accordingly, we assumed the parameters to be $\lambda = 10$ and $k_BT/U_0 \exp(-\lambda) = 0.18$ for all our simulations reported here (see Supplemental Material, Sec. IV, for more details [23]). For the choice of these parameters, the interactions are hard sphere like, felt only by the nearest neighbours. A simulation assembly for $U_{\text{trap}}/k_BT = 112$ is shown in Fig. 2(b), which can be compared with the snapshot [see Fig. 2(d)] of a crystallite formed under similar experimental conditions.

To characterize the structural order of the assemblies, we used the 2D global hexagonal bond-orientational order

parameter $|\psi_6|$, defined as [27] $\psi_6 = \langle (1/N) \sum_{m=1}^{N} \frac{1}{N_b} \sum_{n=1}^{N_b} \exp(6i\theta_{mn}) \rangle$, where N is the total number of particles, N_b is the number of neighbors of the mth particle, and θ_{mn} is the angle between the bond connecting the mth particle with its nth neighbor and a fixed direction in the XY plane. The value of $|\psi_6|$ was estimated to be 0.9 and 0.62 for the simulated and experimental crystallites shown in Figs. 2(b) and 2(d), respectively. The difference of $|\psi_6|$ could be understood by analyzing the local bond-orientational order parameter $\phi_6(m) = (1/N_b) \sum_{n=1}^{N_b} \exp(6i\theta_{mn})$ shown in Figs. 2(c) and 2(e). While the values of $|\phi_6(m)|$ match very well at the center, the outer edges of the experimental crystallites were found to be more disordered. This arose because the experimental trapping potential was flattened out at the edges, implying lower confinement, while the simulated crystal was assumed to be in a harmonic potential. The hexagonal ordering of the crystallite could be observed in the bulk as well as the boundaries, similar to previous work on soft walls [22].

Next, we investigate the dynamics of external impurities (dopants) injected within the crystallites. Experimentally, this was achieved by mixing impurity particles with the colloidal suspension and subsequently forming doped colloidal crystallites under appropriate illumination. The dopants were typically clumped particles derived from the colloidal suspension used to make the crystallites. In the course of our experiments, we have studied dopants with various shapes and sizes (see Supplemental Material, Sec. VI, Movies M3–M7 [23]) and investigated conditions under which the dopants are spontaneously expelled out of the crystallite or remain trapped inside the crystallite over the entire duration of observation(at least 15 min). The experimental methodology was to choose a particular dopant and repeatedly form colloidal crystallites around the dopant (60–80 times), where the main variabilities were the initial position and orientation of the dopant. Two representative examples are shown in Fig. 3(a) (inset), where the dopants were rods of diameter 1 and 2.5 μm, and length 5 and 3.5 μm, respectively. Our observations show rods of commensurate dimensions (diameter 1 μm, the same as that of the beads of the background crystallite) remained trapped (see Movie M5 [23]) in the crystallite by aligning along a crystal line, whereas for rods of incommensurate dimensions (diameter 2.5 μm) the probability of internalization vs spontaneous expulsion was found to depend strongly on the initial position of the dopant. Both experimental [see Movies M3(a)–M3(d) and M4 (a)–M4(c) [23]] and simulation results (see Movies M8 and M9 [23]) for the probability of expulsion of the incommensurate rod, averaged over all angles, has been shown in Fig. 3(a) as a function of r_i, the initial radial position of the center of the rod, for a crystallite containing 100 particles in both cases. We could take into account the difference in optical polarizability arising due to the difference in shape and size between the dopant and the host colloids in our numerical simulations where the dopant was modeled as a collection of host particles in a bead spring model (see Supplemental Material, Sec. V [23]). The agreement between the two sets of results is encouraging. The simulation (see Movie M8 [23]) showed smooth dynamics of the dopant, whereas experiments showed intermittent motion of the dopant, which is related to the roughness in the spatial variation of the confining potential [Fig. 2(a)]. Moreover, the potential flattens out towards the edges, which reduces the speed of the dopant close to the boundary of the crystallite.

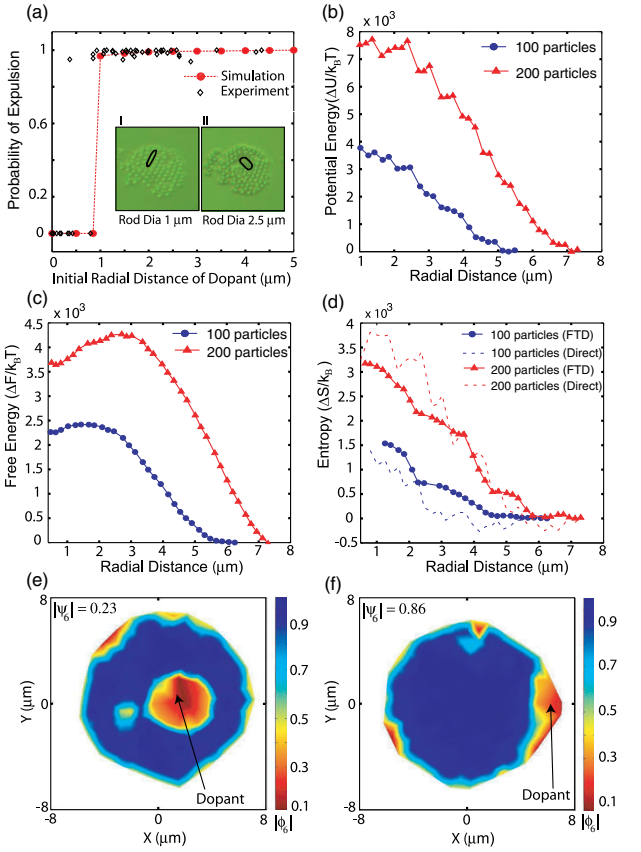

FIG. 3. (a) Comparison of experimental and simulation results for the probability of expulsion as a function of the initial radial position of a dopant shown in inset II, which is a rod of incommensurate size, for a crystal with 100 particles. Inset I corresponds to a commensurate rod as a dopant (see the main text for more details). (b) Potential energy U, (c) free energy F, and (d) entropy S, as a function of the distance of a dopant [corresponding to (a), inset II] from the center of the trap for crystallites with 100 and 200 particles. U, F, and S are calculated relative to their values for the dopant being just outside the crystallite. The entropy calculated from two different methods (see the text) is shown in (d) by full and dashed lines. (e) Theoretical color map of the local bond-orientational order ($|\phi_6|$) when the defect is inside (e) and outside (f) the crystallite.

As a control experiment, we investigated the fate of dopants when the colloidal assembly was in a liquid state and found the dopants to be permanently internalized

(see Movies M10 and M11 [23]). This proved that the results reported here were not caused by a differential optical force between the dopant and host colloids, but rather the crystalline structure of the assembly plays a crucial role in the expulsion of the dopant.

To understand these surprising phenomena, we studied the energetics and thermodynamics of the system using numerical simulations, in which we calculated the potential energy U and the Helmholtz free energy F of the whole system for different positions of the dopant particle inside the crystallite. The free energy was obtained from a calculation of the mean force acting on the dopant as a function of its distance r from the center of the trap. The dopant was fixed at a particular position $\vec{r}$ in the crystallite with the help of an additional constraint [28], and the net force acting on it due to all other particles and the harmonic trap was measured. The mean force was then obtained as an average of the net force over the canonical ensemble. For each value of $\vec{r}$, the system was equilibrated, the average net force $\vec{F}_m$ was measured, and the defect was then moved to the next $\vec{r}$. Finally, the mean force was integrated to obtain the Helmholtz free energy as a function of r_i, the initial distance of the defect particle from the center of the trap:

$$F(r_i) = F(r_0) + \int_{\vec{r}_i}^{\vec{r}_0} \vec{F}_m(\vec{r}) \cdot d\vec{r}.$$

Here, $\vec{r}_0$ is a reference point, taken to be just outside the crystallite (details in Supplemental Material, Sec. V [23]). The energetic and entropic contributions to the free energy were separated using the relation $F = U - TS$. To check thermodynamic consistency, the entropy was also calculated from the temperature derivative of F obtained using finite difference $S(r_i, T) = -[F(r_i, T + \Delta T) - F(r_i, T)]/\Delta T$ with $T = 300$ K and $\Delta T = 22$ K. In Fig. 3(b), the potential energy U of the crystallite for 100 and 200 particles, measured from the value corresponding to the dopant particle being just outside the crystallite, is shown as a function of r_i. The total potential energy is found to decrease monotonically with increasing r_i, although the potential energy of the dopant particle increases as r_i is increased. However, consideration of the potential energy (U) alone is not sufficient to explain the behavior shown in Fig. 3(a). As U is a monotonically decreasing function of r_i, it would predict an expulsion from any initial position of the dopant particle inside the crystallite, contrary to what was experimentally observed. Thus, entropic effects must be taken into consideration in order to explain the experimental observations. The free energy F, measured relative to its value for the dopant particle just outside the crystallite, is shown as a function of r_i in Fig. 3(c). The plot clearly exhibits a peak at a distance r_p from the center. This implies that dopants with initial position $r_i > r_p$ are spontaneously expelled, while those with $r_i < r_p$ would require thermal activation over a free energy barrier, that could be much higher than $k_B T$, in order to come out of the crystallite. This matches with the probability of expulsion of the dopant found in the simulation; e.g., in the 100-particle system, the probability of expulsion showed a sharp rise near $r_i \sim 1$ μm [Fig. 3(a)]. The simulations predict both r_p and the free energy barrier to be lower for smaller number of particles, implying self-purification to become more common as system sizes are reduced.

The origin of the free energy behavior can be understood by considering the total entropy of the system. Figure 3(d) shows the dependence of S, calculated relative to its value for the dopant particle being just outside the crystallite, on r_i. The values of S obtained directly from F and U, as well as the values obtained from the derivative of F with respect to T, are shown to illustrate that the entropy values obtained from two different methods agree within numerical uncertainties. Both the potential energy and the entropy decrease with increasing r_i, but the latter decreases faster for relatively small values of r_i, i.e., $|T\partial S/\partial r| > |\partial U/\partial r|$ for $r_i < r_p$. This causes the free energy to increase initially with increasing r_i, leading to a peak in the free energy at $r_i = r_p$. The dependence of the entropy on r_i may be understood in the following way. The presence of the defect particle disrupts the crystalline order in the assembly, because the dimensions of the defect particle are incommensurate with the crystal. This causes an increase in the total entropy of the system. As the defect particle is moved away from the center, the extent of disruption of the crystalline order decreases, as shown in Figs. 3(e) and 3(f), which depict the spatial distribution of the local bond-orientational order parameter $|\phi_6|$ for two positions of the defect particle in a simulated crystal. The dependence of the extent of crystalline order on the position of the dopant is also evident from the values of the global bond-orientational order parameter $|\psi_6|$, which was smaller (0.23) when the dopant is inside [Fig. 3(e)] compared to its value (0.86) when it is just outside the crystallite [Fig. 3(f)]. This causes the increment of the entropy due to the disruption of crystalline order to decrease with increasing r_i, leading to a reduction of the total entropy. We have seen similar behavior in our experiments where $|\psi_6|$ increases from 0.12 to 0.38 as the rod is expelled out the crystal (details for this and other shapes are available in Supplemental Material, Sec. VI [23]).

To investigate the generality of the phenomena reported here, we investigated the behavior for various values of the system parameters using numerical simulations. The qualitative form of the variation of the free energy as a function of the dopant position was independent of the exact functional form of the assumed interaction potential between the colloidal particles, as long as it is kept as a short-ranged strongly repulsive interaction (see Supplemental Material, Sec. VIII [23]). For dopants of other shapes and sizes (see Supplemental Material, Sec. IX [23]), a free energy maximum could always be

found at a certain distance from the center, although the magnitude of the free energy barrier depended on the dopant dimensions. We have investigated different (nonharmonic) types of external confinement and found (Supplemental Material, Sec. VII [23]) the main conclusions (existence of a free energy barrier) to remain unaltered. Finally, the initial orientation (Supplemental Material, Sec. X [23]) of the dopant inside the crystallite had a small effect on the probability of self-purification.

In summary, we report on an experimental and numerical study of the behavior of dopants injected into confined colloidal crystallites, which showed evidence of position-dependent self-purification. We conclude the internalization of dopants to be primarily driven by gains in the total system entropy, while self-purification is driven by the position dependence of the net potential energy of the dopant-crystallite system, which in turn is intricately dependent on the spatial gradient of the confinement potential. The existence and position of the free energy maximum arises out of a subtle balance between these two competing effects. The studies presented here could be extended to host colloids of higher degree of complexity [10], e.g., nonspherical shapes, self-propelled particles [29], etc., and the insight gained could be useful in designing and assembling new type of soft nanomaterials [30,31].

We thank Soutik Sur, Rituparno Mandal, V. R. Supradeepa, and Arun S for their help with the experiments and simulations and Ajay Sood, Manish Jain, Prabal Maiti, and Srinivasan Raghavan for helpful discussions. The usage of the facilities in Micro and Nano Characterization Facility (MNCF, CeNSE) at IISc, and funding from Science and Engineering Research Board is gratefully acknowledged. This work is partially supported by the Ministry of Communication and Information Technology under a grant for the Centre of Excellence in Nanoelectronics, Phase II.

*ambarish@ece.iisc.ernet.in

[1] P. Leiderer, W. Ebner, and V. B. Shikin, Surf. Sci. **113**, 405 (1982).
[2] V. Vadakkumbatt, E. Joseph, A. Pal, and A. Ghosh, Nat. Commun. **5**, 4571 (2014).
[3] H. Thomas, G. E. Morfill, V. Demmel, J. Goree, B. Feuerbacher, and D. Möhlmann, Phys. Rev. Lett. **73**, 652 (1994).
[4] F. Diedrich, E. Peik, J. M. Chen, W. Quint, and H. Walther, Phys. Rev. Lett. **59**, 2931 (1987).
[5] Q.-H. Wei, C. Bechinger, D. Rudhardt, and P. Leiderer, Phys. Rev. Lett. **81**, 2606 (1998).
[6] J. J. Juarez, P. P. Mathai, J. Alexander Liddle, and M. A. Bevan, Lab Chip **12**, 4063 (2012).
[7] J. J. Juarez and M. A. Bevan, Adv. Funct. Mater. **22**, 3833 (2012).
[8] K. Zahn, J. M. Méndez-Alcaraz, and G. Maret, Phys. Rev. Lett. **79**, 175 (1997).
[9] J. Kyu Cho, Z. Meng, L. Andrew Lyon, and V. Breedveld, Soft Matter **5**, 3599 (2009).
[10] H. Löwen, Eur. Phys. J. Spec. Top. **222**, 2727 (2013).
[11] W. T. M. Irvine, A. D. Hollingsworth, D. G. Grier, and P. M. Chaikin, Proc. Natl. Acad. Sci. U.S.A. **110**, 15544 (2013).
[12] V. W. A. de Villeneuve, R. P. A. Dullens, D. G. A. L. Aarts, E. Groeneveld, J. H. Scherff, W. K. Kegel, and H. N. W. Lekkerkerker, Science **309**, 1231 (2005).
[13] K. Yoshizawa, T. Okuzono, T. Koga, T. Taniji, and J. Yamanaka, Langmuir **27**, 13420 (2011).
[14] Y. Yin, R. M. Rioux, C. K. Erdonmez, S. Hughes, G. A. Somorjai, and A. Paul Alivisatos, Science **304**, 711 (2004).
[15] S. C. Erwin, L. Zu, M. I. Haftel, A. L. Efros, T. A. Kennedy, and D. J. Norris, Nature (London) **436**, 91 (2005).
[16] M. Hermes, E. C. M. Vermolen, M. E. Leunissen, D. L. J. Vossen, P. D. J. van Oostrum, M. Dijkstra, and A. van Blaaderen, Soft Matter **7**, 4623 (2011).
[17] L. J. Moore, R. D. Dear, M. D. Summers, R. P. A. Dullens, and G. A. D. Ritchie, Nano Lett. **10**, 4266 (2010).
[18] J. A. Drocco, C. J. Olson Reichhardt, C. Reichhardt, and B. Janko, Phys. Rev. E **68**, 060401 (2003).
[19] K. Nelissen, B. Partoens, and F. M. Peeters, Phys. Rev. E **69**, 046605 (2004).
[20] B. A. Grzybowski, X. Jiang, H. A. Stone, and G. M. Whitesides, Phys. Rev. E **64**, 011603 (2001).
[21] D. L. J. Vossen, M. A. Plaisier, and A. van Blaaderen, in Proc. SPIE **5514**, 755 (2004).
[22] I. Williams, E. C. Oğuz, R. L. Jack, P. Bartlett, H. Löwen, and C. Patrick Royall, J. Chem. Phys. **140**, 104907 (2014).
[23] See Supplemental Material at http://link.aps.org/supplemental/10.1103/PhysRevLett.117.258002 for description of movies, theoretical analysis and details of the experimental setup, which contains Refs. [24–26].
[24] M. O. Robbins, K. Kremer, and G. S. Grest, J. Chem. Phys. **88**, 3286 (1988).
[25] C. Yong, Chin. Phys. Lett. **20**, 1626 (2003).
[26] Y. Monovoukas and A. P. Gast, J. Colloid Interface Sci. **128**, 533 (1989).
[27] J. Chakrabarti and H. Löwen, Phys. Rev. E **58**, 3400 (1998).
[28] E. Guardia, R. Rey, and J. A. Padró, Chem. Phys. **155**, 187 (1991).
[29] M. C. Marchetti, J. F. Joanny, S. Ramaswamy, T. B. Liverpool, J. Prost, M. Rao, and R. Aditi Simha, Rev. Mod. Phys. **85**, 1143 (2013).
[30] G.-R. Yi, D. J. Pine, and S. Sacanna, J. Phys. Condens. Matter **25**, 193101 (2013).
[31] F. Li, D. P. Josephson, and A. Stein, Angew. Chem., Int. Ed. **50**, 360 (2011).